ELSEVIER

Journal of Materials Processing Technology 121 (2002) 273–284

Journal of Materials Processing Technology

www.elsevier.com/locate/jmatprotec

A study on seamless tube in the planetary rolling process

Chih-Kang Shih, Ray-Quen Hsu, Chinghua Hung*

Department of Mechanical Engineering, National Chiao Tung University, 1001 Ta-Hsueh Road, Hsinchu, Taiwan, ROC

Received 4 February 2001

Abstract

In this paper, the finite element method and the dual-stream functions upper bound method are selected to analyze the tube rolling process with a planetary rolling mill. Three-dimensional elastic–plastic finite element simulations with special emphasis on the determination of the roller profile and realistic contact conditions between the rollers, workpiece and mandrel are used to reveal the deformation characteristics of seamless tube during the rolling process. In addition, the kinematically admissible velocity field of the deforming tube is described in terms of two stream functions so that the velocity components of the deforming tube can be obtained through the upper bound analysis. In both analysis methods, the equation of meshing is used to determine the contact condition between the rollers and the workpiece. The results from both methods with different variables are observed and compared.

Keywords: Planetary rolling process; Finite element; Upper bound; Dual-stream functions

1. Introduction

The planetary rolling mill (Planetenshrägwalzwerk, PSW), as shown in Fig. 1 [1], has been operated successfully in the roughing rolling process. The advantages of PSW include flexibility of workpiece size, low rolling load, low lateral spread of material [2,3] and low temperature drop between the leading and tail ends of the rolled workpiece [4]. Because of its high reduction and continuity, the PSW is also able to manufacture seamless tubes from pierced billets. A set of PSWs used as a elongation mill combined with a sizing or stretch-reducing mill in tube production forms one continuously operating unit (Fig. 2) [5] and permits the omission of the cooling and reheating operations that are usually required after elongation for the conventional elongation mill. Thus cost can be saved because reheating furnaces are not necessary and the noise level is reduced because there are no cold tubes clashing against the mandrel. Further, the PSW provides close wall thickness tolerances through transverse rolling at the elongation stage [6] and increased yield.

The PSW mainly contains three conical rollers, an external ring and a mandrel. As shown in Fig. 3, the rollers are inclined and located equally around the axis of workpiece with their axes intersecting that of the workpiece by an offset angle. This arrangement provides a feed movement as the rollers rotate around the workpiece. The rollers are positioned by the ring, which encloses the rollers and rotates in the direction opposite to that of rollers. Besides fixing the rollers, the main purpose of the ring is to counteract the twisting deformation of the workpiece during the rolling process and to keep the tubes round after rolling.

Most papers about PSW have been focused on the rod rolling process, with only a few on the seamless tube rolling process. For the rod rolling process, Aoyagi and Ohta [7] observed the flow of the material, the load and the torque on the rollers, and the pressure distribution on the rollers during the rolling process with different cross-section reduction ratios. In addition, they studied the influence of the offset angle on the exit velocity of the rods. Nishio et al. [8] discussed the quality characteristics of rolled products with different offset angles and roller profiles. In analytical research, Hwang et al. [9] used dual-stream functions for investigating the plastic deformation behavior of the rod during the planetary rolling process. In numerical analysis, Li [10] used the elastoplastic finite element method to analyze the elementary deformation behavior of the planetary rolling process. Shih and Hung [11] employed three-dimensional finite element analysis and an optimum method to obtained the rolling deformation and the resulting stress and strains. For the tube rolling process, Siebke and Gartner [12] used elementary mechanics to analyze the force acting on the rollers and the mandrel. However, few works have been done on studying the tube rolling process with three-dimensional finite element deformation analysis or with an upper bound solution through dual-stream functions. The purpose of this study is thus to use the finite element method

* Corresponding author. Fax: +886-35-720-634.
E-mail address: chhung@cc.nctu.edu.tw (C. Hung).

0924-0136/02/$ – see front matter
PII: S0924-0136(01)01265-1

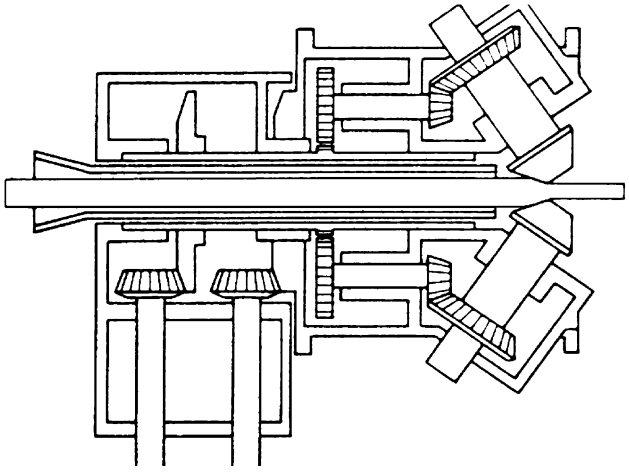

Fig. 1. Cross-section of PSW (source: H. Marten, New approaches in plant technology to increase quality and productivity, MPT Metall. Plant Technol. 9 (5) (1986) 39–55).

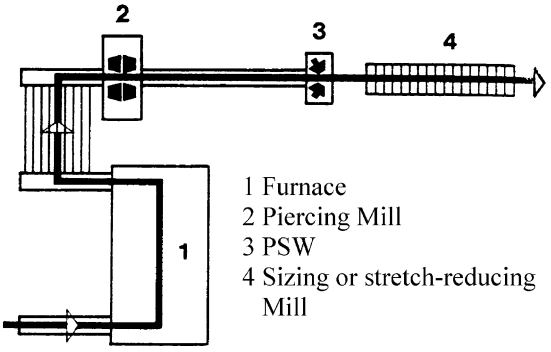

Fig. 2. Layout of a tube production plant with PSW (source: E. Bretschneider, New process for the production of seamless tubes-PSW now also in the tube sector, MPT Metall. Plant Technol. 6 (6) (1983) 44–49).

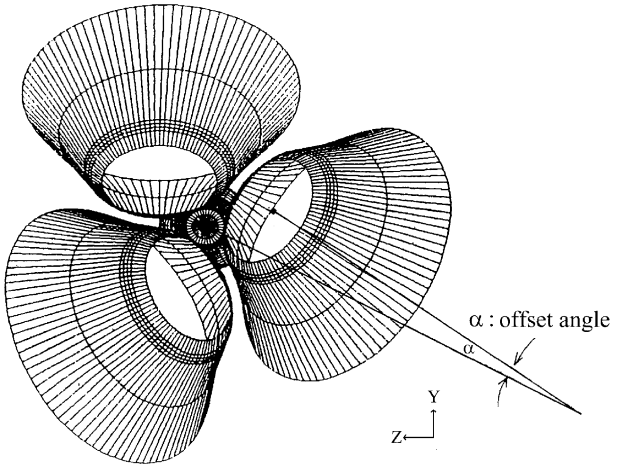

Fig. 3. Rollers of PSW (courtesy of Walsin Cartech Specialty Steel Corporation).

to further analyzes the planetary rolling process with a systematic study of the effects of rolling parameters and also compare the results to those derived from dual-stream functions. Because the simulation of the planetary rolling process is three-dimensional with characteristics of non-linearity and large deformation, the numerical calculation demands efficient and powerful software. The vectorized explicit finite element code LS-DYNA3D [13] has thus been selected as the simulation tool.

2. Mathematical model

2.1. Simplification of the PSW model

The operation of the PSW includes the revolution of three rollers, the rotation of the rollers and the rotation of the external ring. The major boundary conditions include the contacts between three rollers and the workpiece, the contacts between the rollers and the ring and the contacts between the workpiece and the mandrel. Thus, a complete and realistic model will make the finite element analysis very complicated. In addition, the control over the rotation of each component and the analyses of contacts between each component will incur huge computational time. Therefore, it is reasonable to simplify the simulation model. If the axes of the rollers are fixed and the orbital revolution of the rollers is ignored, the external ring can be omitted from the PSW model. The orbital motion provided by the external ring can then be taken care of by the relative motion of the workpiece with free rotational degree of freedom. Thus the key points on the analysis of the simplified model contain only the rotation of the rollers and the contact conditions between the rollers, the workpiece and the mandrel.

2.2. Finite element model

A third-order polynomial was used to define the profiles of the geometry of the rollers. For a point $\boldsymbol{R}_{\mathrm{R}}$ on a roller, the radius r_{R} was defined as

$$r_{\mathrm{R}} = r_{\mathrm{R}}(x) = ax^3 + bx^2 + cx + d \tag{1}$$

Thus the coordinates of $\boldsymbol{R}_{\mathrm{R}}$ on the roller's coordinate system S_{R} can be represented as

$$\boldsymbol{R}_{\mathrm{R}} = [\,x_{\mathrm{R}} \quad y_{\mathrm{R}} \quad z_{\mathrm{R}} \quad 1\,]^{\mathrm{T}} \tag{2}$$

where

$$\begin{aligned} x_{\mathrm{R}} &= ff - u, \qquad y_{\mathrm{R}} = r_{\mathrm{R}} \cos\theta, \\ z_{\mathrm{R}} &= r_{\mathrm{R}} \sin\theta, \qquad ff = \text{const.} \end{aligned} \tag{3}$$

where $0 \le \theta < 2\pi$, $0 \le u < U$, $U = \text{const.}$.

Fig. 4 shows the projective profile of the roller on the local roller's coordinate system. The revolution of this curve with respect to the axis X_{R} makes the complete profile of a roller. The global coordinate system of the simulation model is

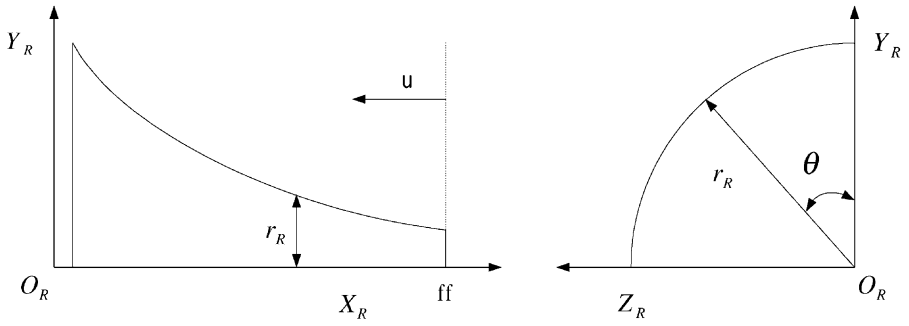

Fig. 4. Roller profile on the coordinate system S_R.

defined as the coordinate system of the workpiece. The geometric relation between the local coordinate system $S_R(X_R, Y_R, Z_R)$ and the global coordinate system $S_0(X_0, Y_0, Z_0)$ is shown in Fig. 5. Thus, a point $\boldsymbol{R}_R$ in S_R can be represented as $\boldsymbol{R}_0$ in S_0 by using the coordinate transformation

$$\boldsymbol{R}_0 = \boldsymbol{M}_{0R}\boldsymbol{R}_R \tag{4}$$

The transformation matrix is

$$\boldsymbol{M}_{0R} = \begin{bmatrix} \cos\beta\cos\alpha & \sin\beta\cos\alpha & -\sin\alpha & 0 \\ -\sin\beta & \cos\beta & 0 & \mathrm{d}r \\ \cos\beta\sin\alpha & \sin\beta\sin\alpha & \cos\alpha & 0 \\ 0 & 1 & 0 & 1 \end{bmatrix} \tag{5}$$

where α represents the offset angle and β represents the inclined angle. Through the transformation matrix $\boldsymbol{M}_{0R}$, point $\boldsymbol{R}_0$ becomes

$$\boldsymbol{R}_0 = [x \quad y \quad z \quad 1]^{\mathrm{T}} \tag{6}$$

$$\begin{aligned} x &= \cos\beta\cos\alpha\, x_R + \cos\alpha\sin\beta\, y_R - \sin\alpha\, z_R, \\ y &= -\sin\beta\, x_R + \cos\beta\, y_R + \mathrm{d}r, \\ z &= \cos\beta\sin\alpha\, x_R + \sin\beta\sin\alpha\, y_R + \cos\alpha\, z_R \end{aligned} \tag{7}$$

With the above procedure, the authors built all three rollers with 120° separation together with a hollow workpiece and a cylindrical mandrel. A complete model was established and then the corresponding mesh system was generated, as shown in Fig. 6.

Low-alloy-contained stainless steel in the tube rolling process was analyzed. The effective stress vs. effective strain curve of 304L stainless steel at 1000 °C as shown in Fig. 7 [14] was adopted as the material property in the finite element analysis. The effective stress is assumed to be constant as the effective strain is greater than 0.7. At high temperature, the material is sticky and the coefficient of friction in the contact surface was taken as $\mu = 0.5$ [15].

2.3. Contact analysis between the roller and the workpiece

By observing the geometrical relationship of the roller and the workpiece it is found that because the surface of the workpiece is formed by a curve rotating around the X_0-axis, the normal vector of any point on the workpiece surface will pass through the center axis. Similar condition prevails in the rollers also. Thus on the contact point, the normal vector must simultaneously pass through the axis of the workpiece and the axis of the roller.

The point $\boldsymbol{R}_R$ is represented as $\boldsymbol{R}_0$ in the coordinate system S_0 (Eqs. (6) and (7)); therefore the normal vector $\boldsymbol{N}$ of $\boldsymbol{R}_0$ is represented as

$$\boldsymbol{N} = \boldsymbol{N}(N_x, N_y, N_z) = \frac{\partial \boldsymbol{R}_0}{\partial u} \times \frac{\partial \boldsymbol{R}_0}{\partial \theta} \tag{8}$$

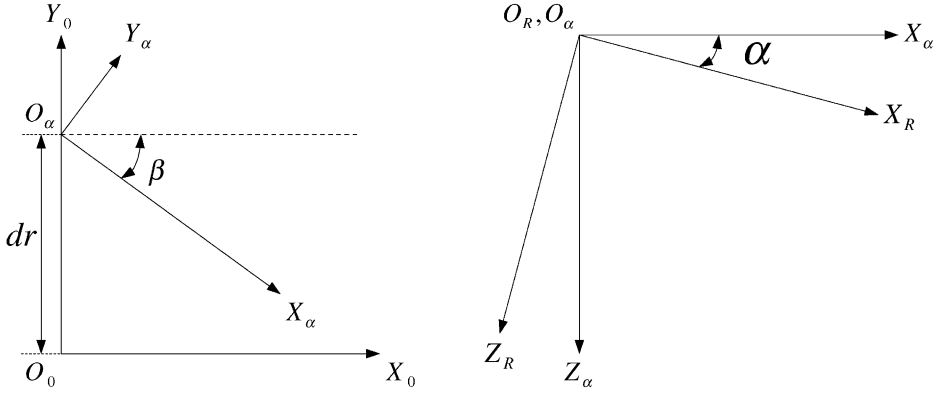

Fig. 5. Relation between roller coordinate system and workpiece coordinate system.

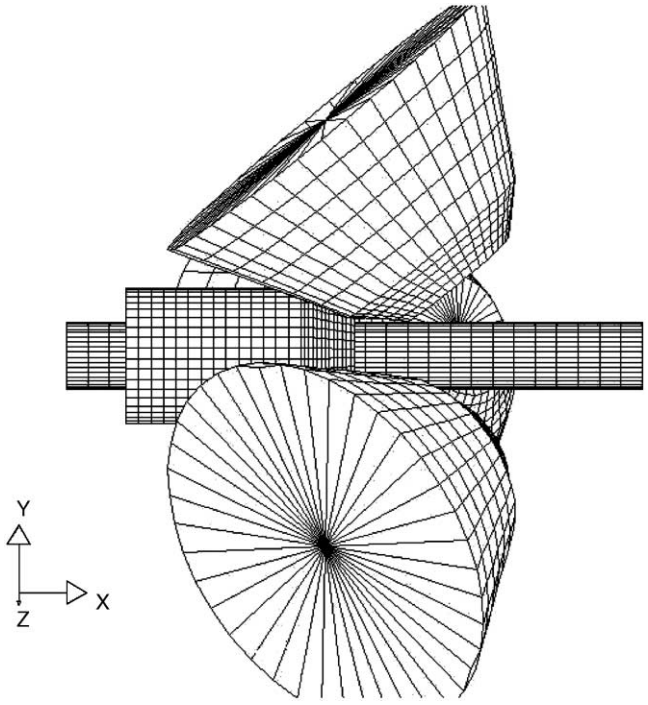

Fig. 6. Mesh system of PSW.

Assume that $\boldsymbol{R}_0$ is the contact point between the roller and the workpiece and that the corresponding normal vector extends through point M on the axis of the workpiece. The coordinate of M is

$$\boldsymbol{M} = [\,x_m \quad 0 \quad 0 \quad 1\,]^{\mathrm{T}} \tag{9}$$

where x_m is a constant.

Thus the vector from $\boldsymbol{M}$ to $\boldsymbol{R}_0$ can be written as

$$\frac{x_m - x}{N_x} = \frac{0 - y}{N_y} = \frac{0 - z}{N_z} \tag{10}$$

so that

$$f(u, \theta) = N_z y - N_y z = 0 \tag{11}$$

The equation above is called the equation of meshing [16]. From Eq. (11), we have

$$y = z\frac{N_y}{N_z} \tag{12}$$

If there exists $x_m = x(u)$, the corresponding θ, y and z can be obtained. Then the distance from the contact point to the axis of workpiece is

$$r_m = \sqrt{(y^2 + z^2)} = |z| \sqrt{1 + \left(\frac{N_z}{N_y}\right)^2} \tag{13}$$

By connecting each contact points, a contact line can be obtained. Rotating this contact line around the axis of workpiece, generates a special profile for the workpiece, which can perfectly fit to the roller through contact. A similar procedure can be used to derive a special profile of roller if the deformation of the workpiece is pre-given.

2.4. Dual-stream functions

The upper bound method in which velocity components are derived from dual-stream functions is used in the following analysis. The concept that an admissible velocity field for an incompressible body in a three-dimensional space can be represented in terms of two stream functions

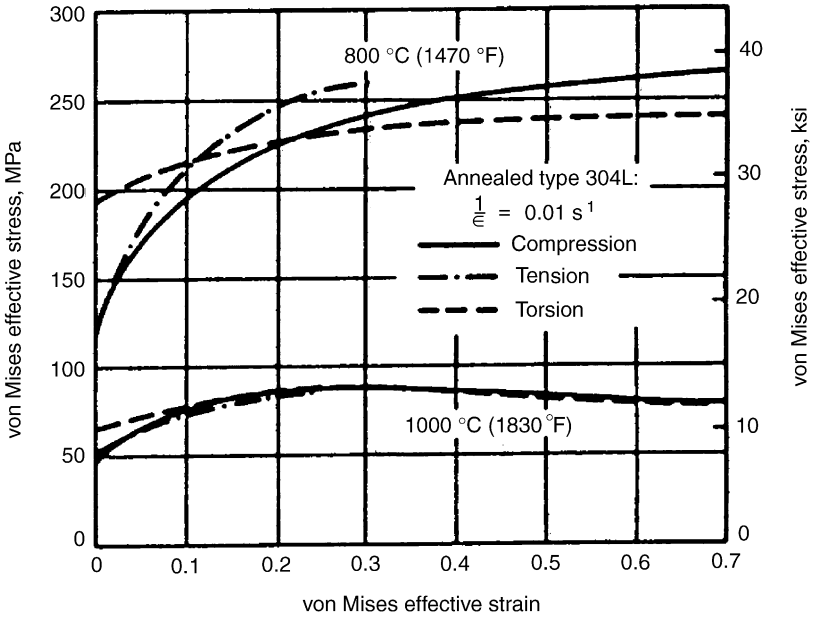

Fig. 7. Effective stress–effective strain curve of 304L stainless steel (source: H.E. Boyer, Atlas of Stress–Strain Curves, American Society of Metals, Metals Park, OH, 1987, p. 301).

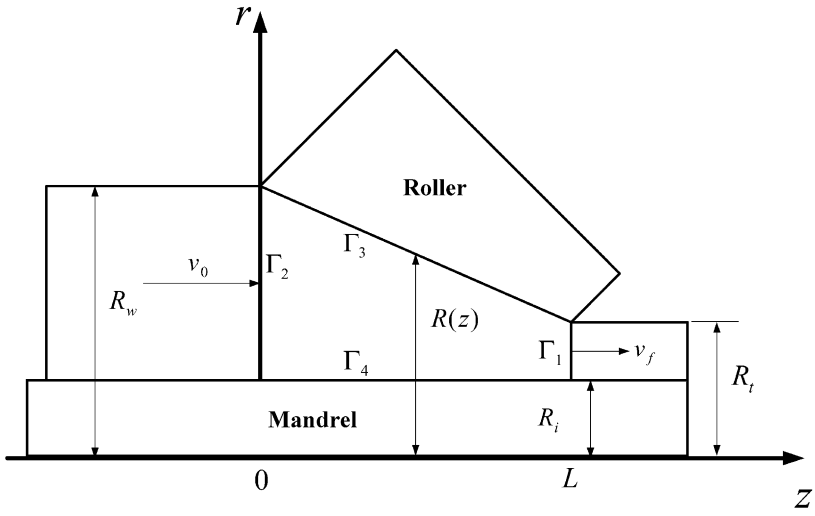

Fig. 8. The tube, the roller and the mandrel.

was first proposed by Nagpal [17]. The velocity components in cylindrical coordinates can be written as the cross-product of the gradients of two stream functions:

$$\boldsymbol{V} = \boldsymbol{V}(V_r, V_\theta, V_z) = \nabla\psi \times \nabla\phi \tag{14}$$

where ψ and ϕ are the stream functions and (V_r, V_θ, V_z) are the velocity components.

The velocity field can be determined by choosing a flow function that makes the tool boundary a stream function [18]. In this paper, the rollers are considered rigid and the material properties of hollow tubes as rigid–plastic and isotropic. Thus the flow pattern of the deforming material in the r–z-plane can be written as [19] (Fig. 8)

$$\phi = v_0 \frac{R_w^2 - R_i^2}{2} \frac{r^2 - R_i^2}{R(z)^2 - R_i^2} \tag{15}$$

where $R(z)$ represents the workpiece profile in the roll gap and can be defined (Fig. 9) as

$$R(z) = R_1(z) + R_2(z) \tag{16}$$

The workpiece in the roll gap is divided equally into three parts corresponding to the three rollers, Fig. 9 showing the configuration of one of such parts. In the figure, R_1 represents the deforming profile, which is deformed by the roller and can be obtained from the equation of meshing, whilst R_2 denotes the free surface of the deforming workpiece.

The contact (deforming) area can be determined from the intersection of two rigid bodies. By assuming that both the roller and the workpiece are rigid, the interfered geometry can be derived once the workpiece is positioned with respect to the roller. The range of interference can be represented in terms of two curves, i.e., C_U and C_L in Fig. 9. Thus, the corresponding θ_{C_L} and θ_{C_U} can be obtained and can then be represented as functions of z.

In the θ–r-plane, the flow pattern is assumed to be that the circumferential velocity along the radius direction is linearly distributed [9] and can be written as

$$\psi = \frac{z}{l} - \frac{\theta}{2\pi} \tag{17}$$

where l is the moving distance along the z-axis as the hollow tube makes a complete rotation.

Then the velocity components in cylindrical coordinates can be derived from Eqs. (14), (15) and (17) as

$$V_r = \frac{v_0}{2} \frac{(r^2 - R_i^2)(R_w^2 - R_i^2)R(z)}{(R(z)^2 - R_i^2)^2 r\pi} \left(\frac{\partial R(z)}{\partial z}\right),$$
$$V_\theta = v_0 \frac{(R_w^2 - R_i^2)r}{(R(z)^2 - R_i^2)l}, \qquad V_z = \frac{v_0}{2\pi} \frac{R_w^2 - R_i^2}{R(z)^2 - R_i^2} \tag{18}$$

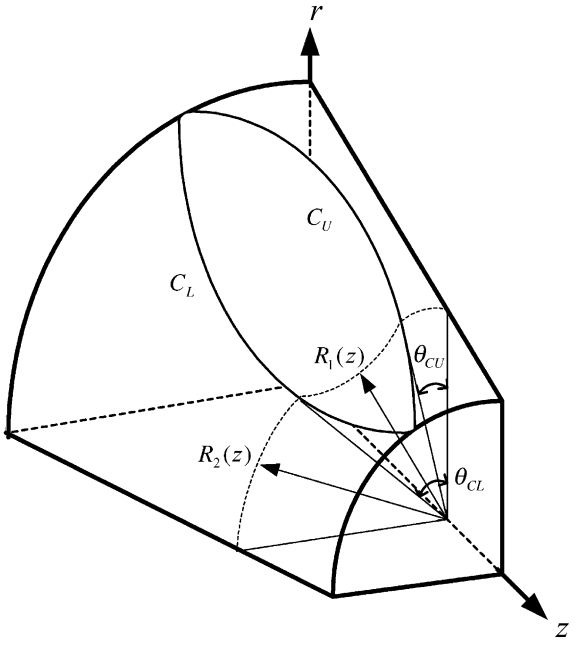

Fig. 9. A workpiece in the roll gap.

The strain rates derived from Eq. (18) are

$$\dot{\varepsilon}_{rr} = \frac{\partial V_r}{\partial r} = \frac{v_0}{2}\frac{(R_w^2 - R_i^2)R(z)(r^2 + R_i^2)}{\pi(R(z)^2 - R_i^2)^2 r^2}\left(\frac{\partial R(z)}{\partial z}\right),$$

$$\dot{\varepsilon}_{\theta\theta} = \frac{1}{r}\frac{\partial V_\theta}{\partial \theta} + \frac{V_r}{r} = \frac{v_0}{2}\frac{(R_w^2 - R_i^2)(r^2 - R_i^2)R(z)}{(R(z)^2 - R_i^2)^2 r^2 \pi}\left(\frac{\partial R(z)}{\partial z}\right),$$

$$\dot{\varepsilon}_{zz} = \frac{\partial V_z}{\partial z} = -v_0\frac{(R_w^2 - R_i^2)R(z)}{(R(z)^2 - R_i^2)^2\pi}\left(\frac{\partial R(z)}{\partial z}\right) \tag{19}$$

and, from Eq. (19):

$$\dot{\varepsilon}_{rr} + \dot{\varepsilon}_{\theta\theta} + \dot{\varepsilon}_{zz} = 0 \tag{20}$$

showing that volume constancy is satisfied and the constructed velocity field is kinematically admissible.

2.5. Upper bound solution

Among all kinematically admissible velocity fields, the actual one minimizes the expression [20]

$$J^* = \frac{2}{\sqrt{3}}\sigma_0\int_V\left(\frac{1}{2}\dot{\varepsilon}_{ij}\dot{\varepsilon}_{ij}\right)^{1/2}\mathrm{d}V + \int_{S_\mathrm{V}}\tau|\Delta v|\,\mathrm{d}S - \int_{S_\mathrm{t}} T_i v_i\,\mathrm{d}S \tag{21}$$

The first term on the right-hand side is the internal strain energy rate in the deformation zone, whilst the second term accounts for the shear loss within the material over the surface of velocity discontinuities Γ_s and the friction loss dissipated on the contact surfaces Γ_f. It can be represented as

$$\int_\Gamma \tau|\Delta v_\Gamma|\,\mathrm{d}S = \frac{1}{\sqrt{3}}\int_{\Gamma_\mathrm{s}}\sigma_0|\Delta v_{\Gamma_\mathrm{s}}|\,\mathrm{d}S + \frac{m}{\sqrt{3}}\int_{\Gamma_\mathrm{f}}\sigma_0|\Delta v_{\Gamma_\mathrm{f}}|\,\mathrm{d}S \tag{22}$$

where $\Delta v_{\Gamma_\mathrm{s}}$ and $\Delta v_{\Gamma_\mathrm{f}}$ are the velocity discontinuities across the boundary surfaces and m denotes the friction factor on the contact surface. The velocity discontinuity $\Delta v_{\Gamma_\mathrm{s}}$ along Γ_1 and Γ_2 can be represented as Δv_1 and Δv_2:

$$\Delta v_1 = V_r|_{z=L} = \frac{v_0}{2r\pi}\frac{(r^2 - R_i^2)(R_w^2 - R_i^2)R_0}{(R_0^2 - R_i^2)^2}\left(\frac{\partial R(L)}{\partial z}\right) \tag{23}$$

$$\Delta v_2 = V_r|_{z=0} = \frac{v_0}{2r\pi}\frac{(r^2 - R_i^2)R_w}{R_w^2 - R_i^2}\left(\frac{\partial R(0)}{\partial z}\right) \tag{24}$$

and $\Delta v_{\Gamma_\mathrm{f}}$ along Γ_3 and Γ_4 are written as Δv_3 and Δv_4:

$$\Delta v_3 = \sqrt{V_r^2 + V_z^2}\Big|_{r=R(z)} = \frac{v_0}{2\pi}\frac{R_w^2 - R_i^2}{R(z)^2 - R_i^2}\sqrt{1 + \left(\frac{\partial R(z)}{\partial z}\right)^2} \tag{25}$$

$$\Delta v_4 = V_z - v_0 \tag{26}$$

The last term in Eq. (21) is the additional power to overcome the back-pull of the tube, which is written as

$$\int_{S_\mathrm{t}} T_i v_i\,\mathrm{d}S = \pi(R_w^2 - R_i^2)\sigma_{xb} \tag{27}$$

It is assumed that $\sigma_{xb} = 0.3\sigma_0$ [9].

3. Discussions of simulation results

3.1. Contact analysis

The profile of a typical PSW roller is described by two straight lines as shown in Fig. 10(a). Fig. 10(b) shows the contact profile of the workpiece corresponding to this roller. The inclination and offset of the roller lead to a V-shape profile for the workpiece. In reality, the right-side part of the V-shape will never occur, instead, a horizontal straight line will replace it because that represents the part of workpiece that had undergone deformation. If the cross-section of the roller is described as in Fig. 10(c), the generated profile of the workpiece will be a straight line as in Fig. 10(d).

The front part of the roller usually will not contact with the deformed workpiece during rolling. The remaining part of the roller, which deforms the workpiece through contact, is called the deforming zone [4]. The roller can be arranged in such a way that makes the deformed workpiece remain constrained by the front part of the roller and the workpiece will then move forward smoothly before departing from the roller. This special front part of roller is then called the smoothing zone.

Based on this characteristic, the front part profile of the roller can be modified by using the equation of meshing, to make the smoothing zone perfectly fit to the deformed workpiece to assure the accurate radius of the workpiece through the rolling process.

3.2. Results of finite element analysis

The vertical cross-section of a deforming tube and its configuration are shown in Figs. 11 and 12, respectively. The workpiece was twisted by the interaction of the rollers and the mandrel, and thus has spiral marks on its surface. Due to the rotation and feed movement brought about by the rollers, the material flow was not uniform between the internal and external part of the tube. The flow velocity on the external part is faster than that near to the mandrel.

Figs. 13 and 14 are the contours of the effective stress and effective strain of the workpiece during the rolling process. It can be seen that the maximum von Mises stress occurs at the parts contacting with the rollers. The largest deformation occurs in the part of the tube where the rolling began, as indicated by the effective strain contours.

For this analysis, the wall thickness of the tube was reduced from 100 mm to five different sizes with the rotational speed of the roller kept at 150 rpm. The inclined angles were set to 50°, which is the typical value for industrial practice. The offset angle of the roller has important effects upon the tube rolling process, especially on the exit velocity of the deformed workpiece.

Fig. 15 shows that the exit velocity increased with the magnitude of the offset angle and decreased with respect to the wall thickness of the deformed tube. In addition, the

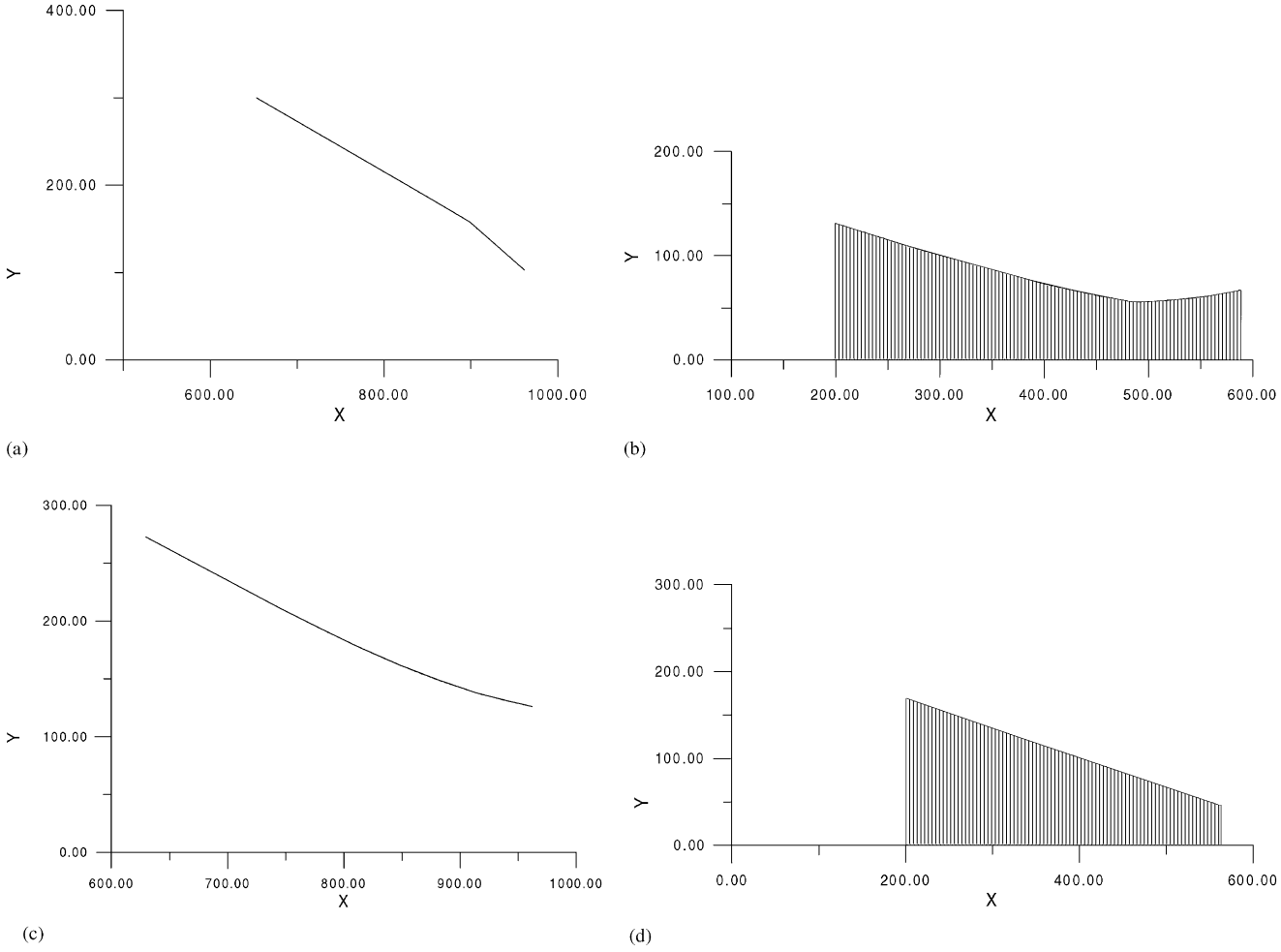

Fig. 10. The roller profile and the generated front end profile of the workpiece (unit: mm): (a) typical roller profile; (b) generated workpiece profile; (c) a roller profile; (d) the workpiece profile generated from (c), where $y = 1.57874 \times 10^{-6}x^3 - 0.00326815x^2 + 1.71973x + 90.9101$.

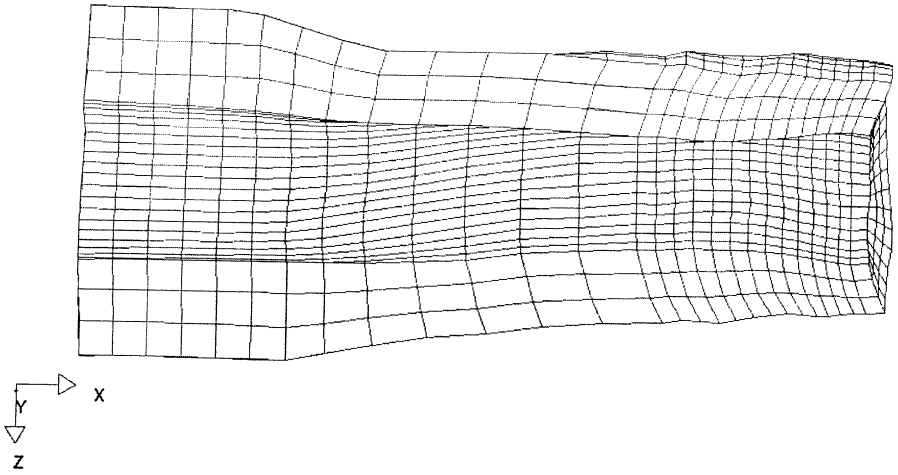

Fig. 11. Cross-section of the deforming tube.

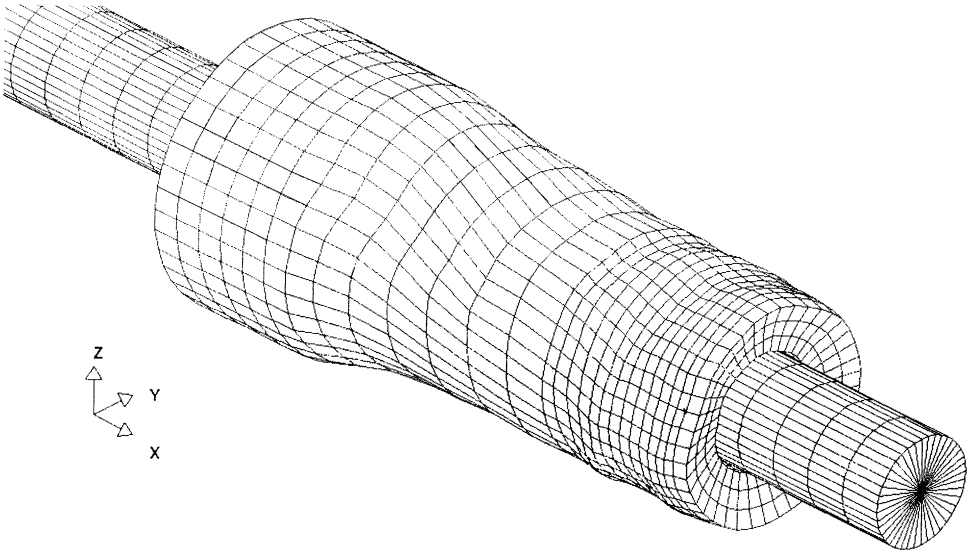

Fig. 12. Configuration of the deforming tube.

rolling load increased with the offset angle and also increased with the tube thickness, as shown in Fig. 16.

3.3. Results of upper bound approach

Velocity components obtained from dual-stream functions are shown in Fig. 17(a) while Fig. 17(b) shows the velocity components on the tube surface from the finite element analysis. The velocity distribution from the dual-stream functions clearly indicates the rotational movement of the workpiece: similar results are found in the finite element calculation. However, the amount of advancing movement of the deforming tube is not as obvious as that obtained from finite element analysis. The energy rates calculated from the dual-stream functions are displayed in Fig. 18 and are compared with the results from the finite element analysis. The tendencies from both analyses are very similar, as shown in the figure. The energy dissipation rates all increase with the reduction of cross-sectional area.

The differences between the two methods of analysis come mainly from the oversimplified assumptions of the dual-stream functions. In fact, the material flow on the roll gap is not uniform, as can be seen in Figs. 11 and 12. The circumferential velocity along the radius direction should not be treated as a linear distribution, especially in the deforming zone. In addition, the lack of consideration of the velocity discontinuities along the interface between the

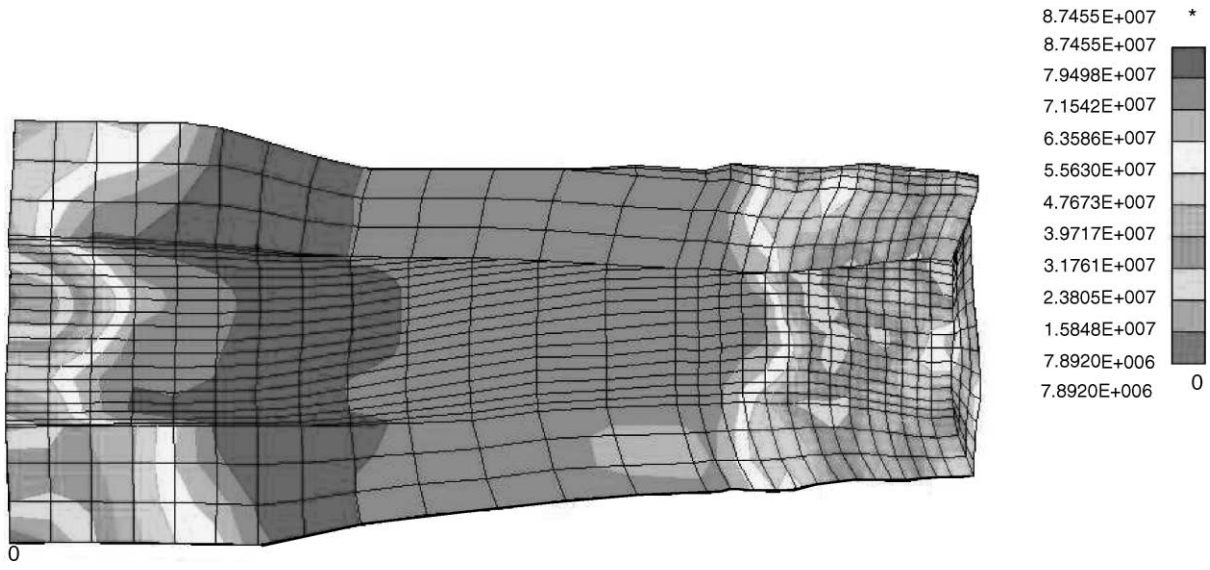

Fig. 13. Distribution of von Mises stress in the deforming tube (unit: Pa).

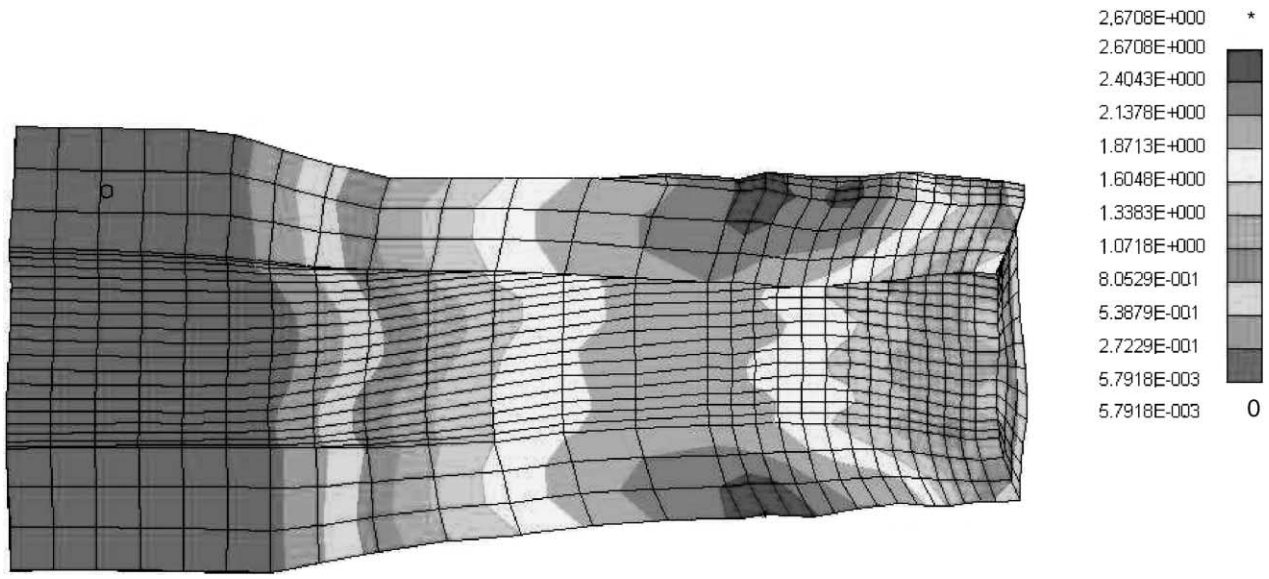

Fig. 14. Distribution of effective strain in the deforming tube.

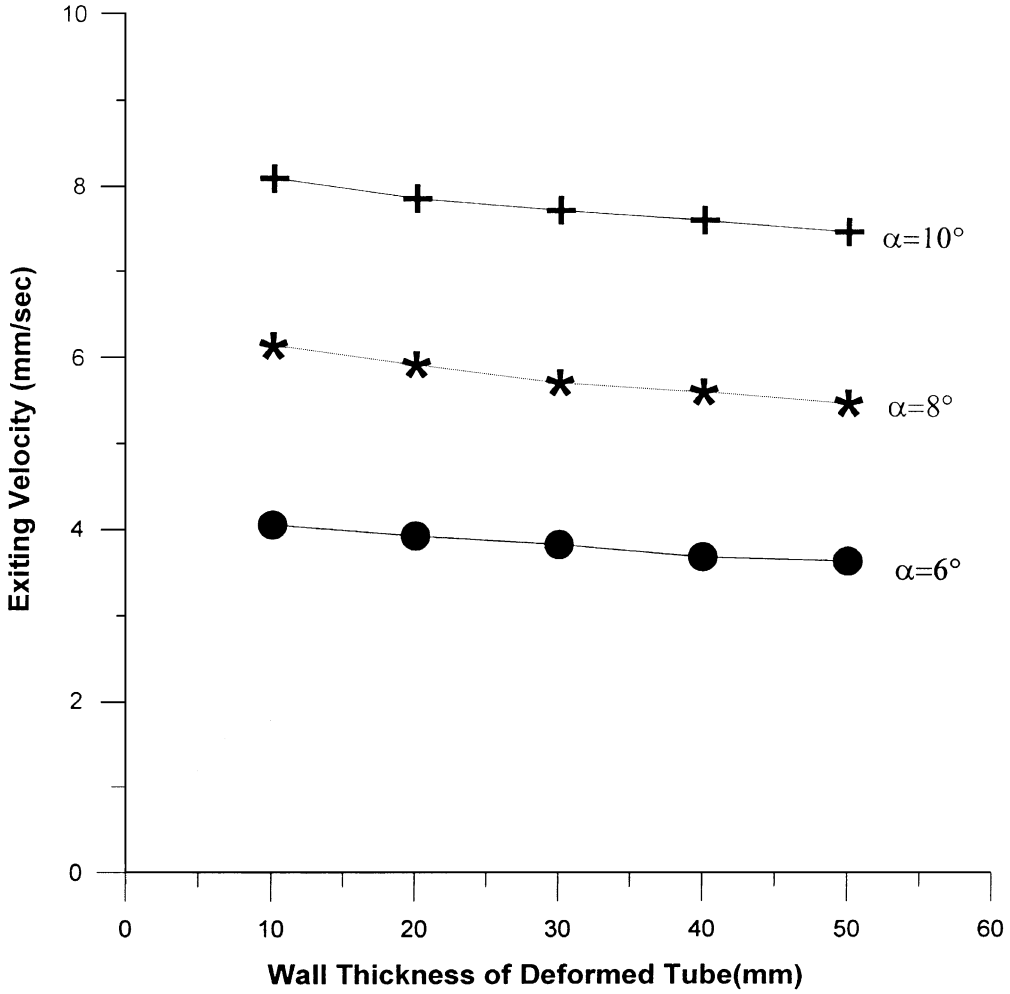

Fig. 15. Relation between the offset angle and the exit velocity of the workpiece.

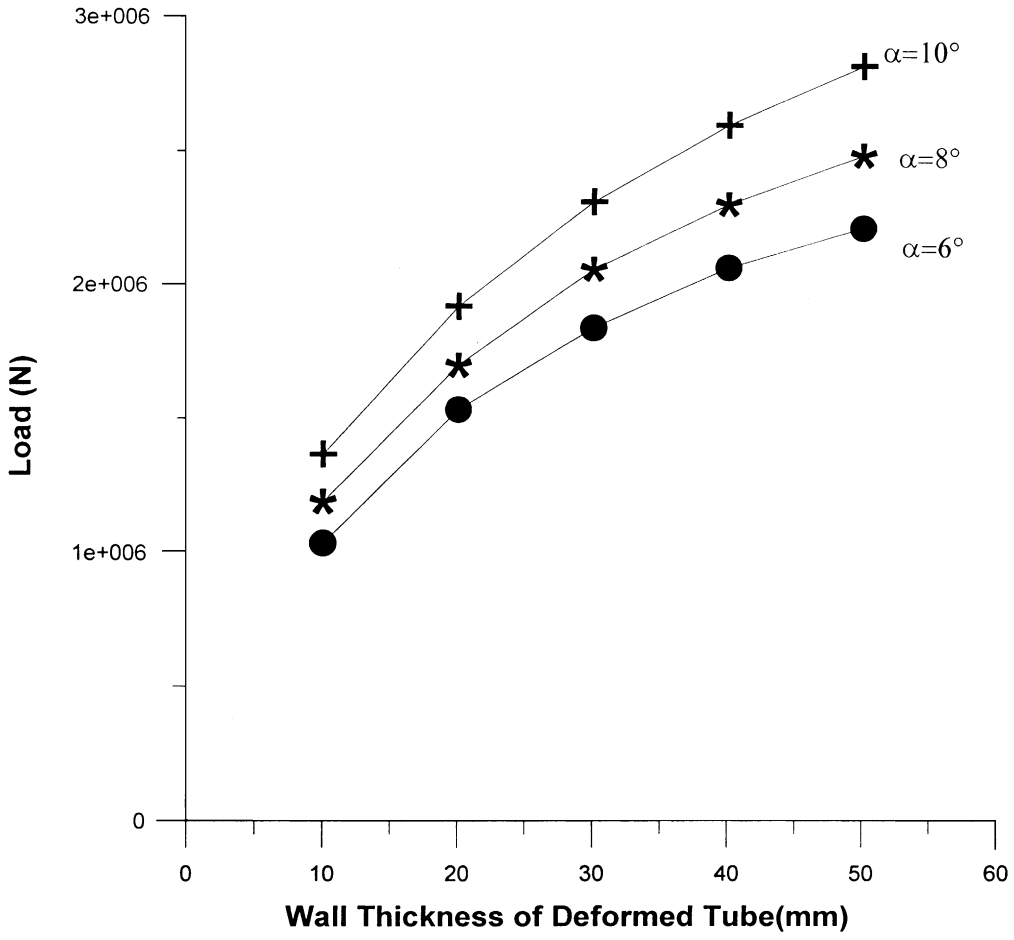

Fig. 16. Relation between the offset angle and the rolling load.

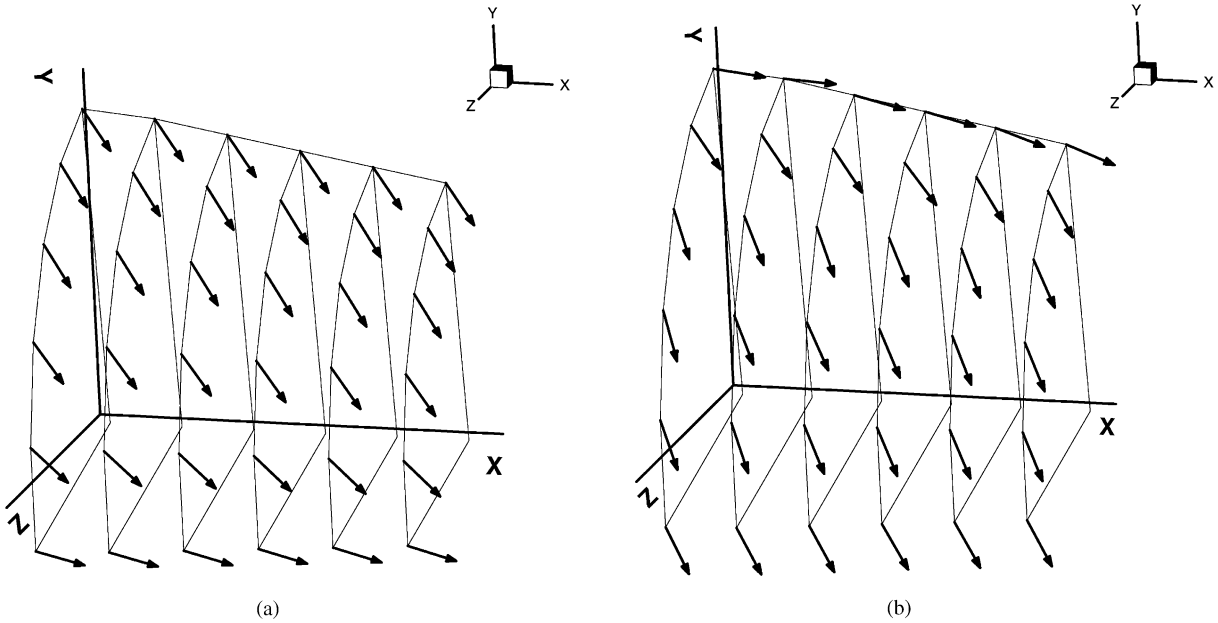

(a) (b)

Fig. 17. Velocity field of the roll gap: (a) upper bound approach; (b) finite element analysis.

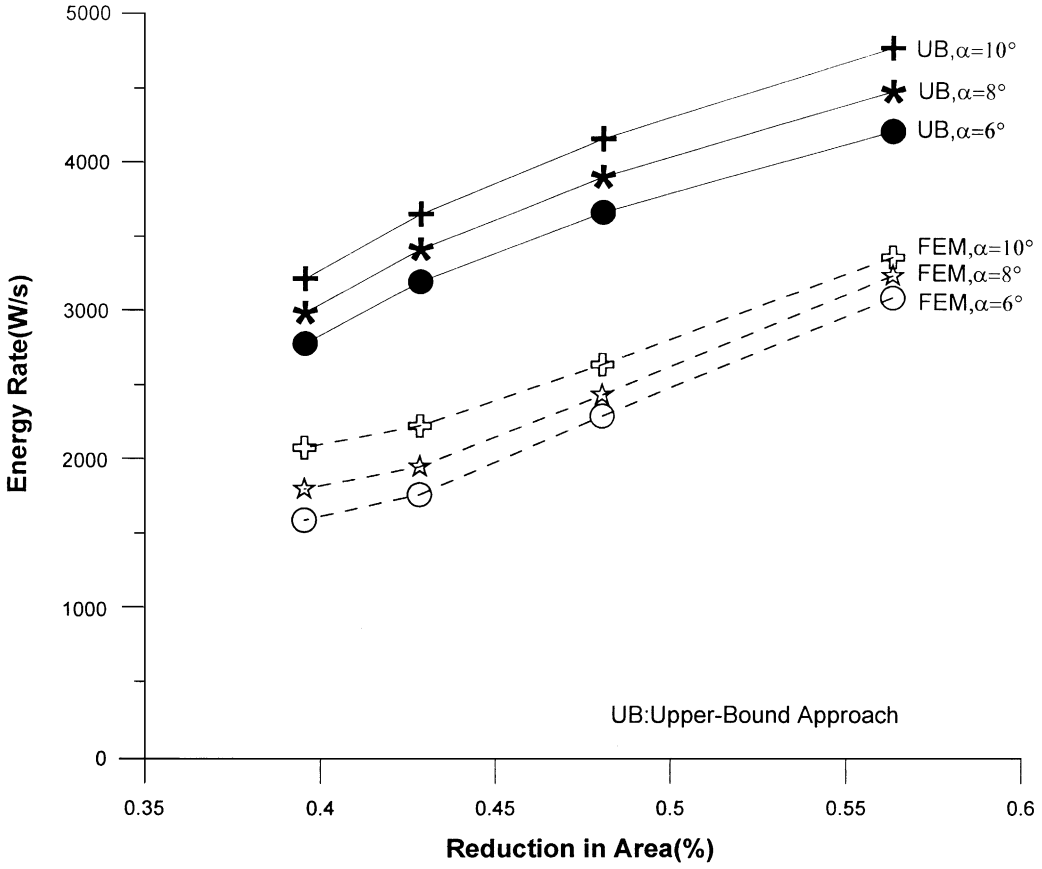

Fig. 18. Energy rate.

deforming surface and the free surface in the roll gap also leads to deviations from the finite element simulation.

4. Conclusions

Applying the PSW in the tube rolling process could help in increasing the working efficiency and obtaining economical benefits. This research tried to provide the solutions of the problem in the planetary rolling process for tube production by using both the finite element method and dual-stream functions. The conclusions are as follows:

1. The geometric model of PSW has been built by using the coordinate transformation method. In addition, the finite element simulation model has been reasonably simplified to help in reducing the complexity of the model and the computational cost.
2. The equation of meshing was adopted to generate the profile of the workpiece that contacts perfectly with the roller and vice versa. It was also used as the tool boundary to define the velocity field for the dual-stream function.
3. The offset angle of the roller influences the exit velocity of the workpiece, the rolling load and the dissipated energy in deformation. Increasing the offset angle can increase the efficiency of the rolling process, but can increase the rolling load and energy dissipation at the same time.
4. Combining the dual-stream functions and upper bound approach provides a feasible way to analyze three-dimensional metal-forming problems analytically. The results show similar tendencies with those from the finite element method in respect of the energy rate, but with some discrepancies in magnitude.
5. The model of the dual-stream function from which the velocity field is derived can be modified further to approach the behavior of the real material during deformation.

References

[1] H. Marten, New Approaches in plant technology to increase quality and productivity, MPT Metall. Plant Technol. 9 (5) (1986) 39–55.
[2] W.J. Ammerling, H. Brauer, Application of 3-roll technology for rolling specialty rod and bar products, Iron and Steel Engr. 65 (9) (1988) 22–27.
[3] W.J. Ammerling, Kocks 3-roll technology for high precision specialty rod and bar product, MPT Metall. Plant Technol. 12 (6) (1989) 14–19.
[4] C. Recalcati, C. Ventura, W. Rensch, HRM high-reduction rolling machine, Wire Ind. 57 (673) (1990) 31–34.

[5] E. Bretschneider, New process for the production of seamless tubes-PSW now also in the tube sector, MPT Metall. Plant Technol. 6 (6) (1983) 44–49.
[6] E. Bretschneider, Novel tube-rolling process using the 3-roll planetary mill (PSW), Iron and Steel Engr. 58 (10) (1981) 51–54.
[7] K. Aoyagi, K. Ohta, Material deformation, rolling load and torque in 3-roll planetary mill, J. JSTP 24 (273) (1983) 1039–1047.
[8] T. Nishio, T. Noma, S. Karashige, H. Hino, T. Tsuta, K. Kadota, Development of three-roll planetary mill (PSW), Kawasaki Steel Tech. Rep. 84 (1995) 81–90.
[9] Y.M. Hwang, H.H. Hsu, G.Y. Tzou, A study of PSW rolling process using stream functions, J. Mater. Process. Technol. 80–81 (1998) 341–344.
[10] Y.J. Li, Elastoplastic analysis of high reduction machine of 3-roll planetary mill by the finite element method, Master Thesis, National Sun Yat-sen University, ROC, 1995.
[11] C.K. Shih, C. Hung, The finite element analysis on planetary rolling process, in: Proceedings of the 23rd National Conference of Theoretical and Applied Mechanics, Taiwan, ROC, 1999.
[12] T. Siebke, H. Gartner, Development of and trials with a seamless tube rolling process employing a 3-roll planetary mill (PSW), MPT Metall. Plant Technol. 13 (2) (1990) 72–80.
[13] J.O. Hallquist, LS-DYNA3D Theoretical Manual, Livermore Software Technology Corporation, 1991.
[14] H.E. Boyer, Atlas of Stress–Strain Curves, American Society of Metals, Metals Park, OH, 1987, p. 301.
[15] E.M. Mielnik, Metalworking Science and Engineering, McGraw-Hill, New York, 1993.
[16] F.L. Litvin, Gear Geometry and Applied Theory, Prentice-Hall, Englewood Cliffs, NJ, 1994.
[17] V. Nagpal, On the solution of three-dimensional metal-forming process, ASME J. Eng. Ind. 99 (1977) 624–629.
[18] V. Nagpal, General kinematically admissible velocity fields for some axisymmetric metal-forming problems, ASME J. Eng. Ind. 96 (1974) 1197–1201.
[19] K.T. Chang, J.C. Choi, Upper-bound solutions to tube extrusion problems through curved dies, ASME J. Eng. Ind. 94 (1972) 1108–1111.
[20] B. Avitzur, Metal Forming, Marcel Dekker, New York, 1980.